Hindawi
Advances in Civil Engineering
Volume 2020, Article ID 8890672, 9 pages
https://doi.org/10.1155/2020/8890672

Research Article

The Bearing and Breakage Characteristics of Crushed Stone Aggregates in the Bedding Course of Permeable Roads

Zhongbing Cai [1,2] **and Chengchun Qiu** [1]

[1]*College of Civil Engineering, Yancheng Institute of Technology, Yancheng, Jiangsu 224051, China*
[2]*School of Science, Nanjing University of Science & Technology, Nanjing 210094, China*

Correspondence should be addressed to Zhongbing Cai; c_zhongbing@ycit.edu.cn

Received 19 August 2020; Revised 23 September 2020; Accepted 7 October 2020; Published 28 October 2020

Academic Editor: Hualei Zhang

The current study of permeable roads helps address urban flooding in Chinese cities caused by frequent heavy rainfall and build smart cities with sponge-like functionality. Crushed stone is widely used in constructing the bedding course of permeable roads because it has good water permeability. Experiments on the compaction of crushed stone were carried out by considering the impact of particle size and gradation to examine the strength and particle breakage characteristics of crushed stone and evaluate its use as the aggregate in the bedding course of permeable roads. The compaction process can be divided into two stages, i.e., the preliminary compaction stage and the particle crushing and intensive compaction stage. The latter consists of an alternating cycle of compacting and crushing. The particle size distribution after crushing can be described analogously to the Talbot continuous gradation equation. Single particle size samples are subject to earlier and stronger particle breakage than the mixed particle size sample, which are affected by both compaction level and loading speed. This study has important application value, and it provides experimental support for the study of materials for urban permeable roads.

1. Introduction

The National Meteorological Center of China Meteorological Administration issued multiple rainstorm yellow alerts since July 2020, and flooding has ravaged the streets of many Chinese cities (Figure 1). There is a rising demand for sponge-like smart cities [1–3], the construction of which requires permeable roads as their underpinning. In fact, permeable roads are massively built throughout the world since the 1980s to prevent urban flooding.

German started the research and development of permeable roads since 1980 and intends to convert >95% of its roads to permeable roads in the early 21st century. The Kinki area of Japan began to install permeable pavements in 1993, and presently in Japan, permeable pavements are widely used in major and minor roads, branch roads, express roads, pedestrian streets, and outdoor spaces (e.g., plazas and parks). China introduced the concept of permeable road in the 1990s and gradually began its application in major cities since 2000. The "Engineering Technical Code for Rain Utilization in Building and Sub-District"(GB50400-2006) issued in 2007 gave regulations on the design, construction, and management of permeable roads [4].

Meng et al. [5] conducted a field survey on the permeability of permeable roads in Shanghai to summarize their application and analyze the factors affecting the actual permeability. Liu [6] studied permeable roads with regard to structural type, road performance, etc. Lu et al. [7, 8] devised a permeameter to investigate the flow characteristics of permeable pavement mixtures under different hydraulic gradient. The results show that Darcy's law is not applicable to analyzing the directional water transport of permeable pavement materials. Instead, the Reynolds number of permeable pavement materials increases with rising hydraulic gradient, and the water flows in permeable pavement materials transition from Darcy flow to non-Darcy flow. Wang [9] summarized the advantages of permeable concrete pavement and analyzed the factors affecting its mechanical

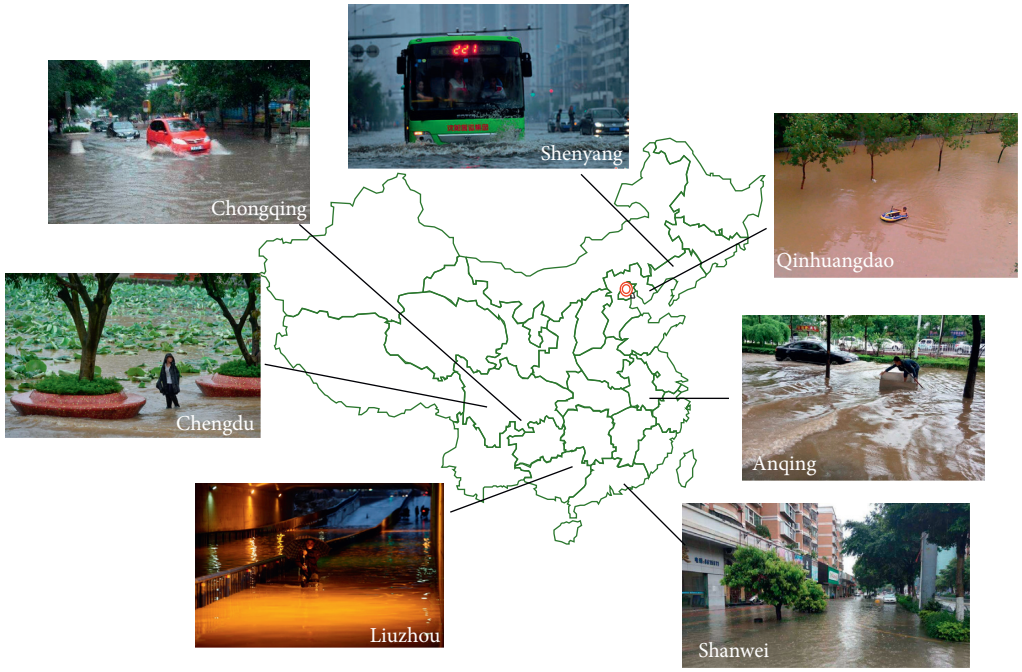

Figure 1: Flooding ravaged in many Chinese cities.

strength, e.g., aggregate particle size, water-binder ratio, silica fume, adhesive layer strength, and method of the forming process. Borgwardt et al. [10, 11] studied the long-term permeability of permeable concrete and brick pavements on-site. They found that permeability depends on the joint material, and permeability is noticeably better when larger aggregates are used.

These prior works demonstrate that the permeability of roads relies heavily on the particle size and gradation of the aggregates. Nevertheless, it must be noted that aggregates can be crushed when they are subject to pressure. Few studies investigated the road bearing ability affected by the crushing of aggregates.

Crushed stone is widely used in constructing the bedding course of permeable roads because it has good water permeability, allows smooth transition of diffusive stress and load, and is readily available and can be obtained locally. This work studied the compaction performance and particle breakage characteristics of crushed stone as the aggregate of permeable roads and analyzed how they are influenced by particle size, gradation, etc. This study can provide experimental support for the study of materials for urban permeable roads, help address urban flooding in Chinese cities caused by frequent heavy rainfall, and can help build smart cities with sponge-like functionality.

2. Compaction Test of Crushed Stone Aggregate

2.1. Equipment. The compaction test system of crushed stone aggregate (Figure 2) includes a home-made compaction device, a loading system, and a data acquisition system. The compaction device is composed of a hollow piston, a cylinder tube, a bottom plate, and other components. The cylinder is 400 mm in height and has an inner and outer diameter of 160 and 180 mm, respectively. The hollow piston is 250 mm in height. The loading system is a WDW-100D universal electronic testing machine produced by the Jinan Huaxin Yuanda Test Equipment Co., Ltd., which has a maximum testing force of 100 kN with a control accuracy of 1% for testing force, displacement, and speed. During the test, the compaction device was placed in the lower chamber of the WDW-100D testing machine, and the load was applied as the indenter on the testing machine which pressed the hollow piston cover.

2.2. Sample Preparation. Test samples were prepared with broken mudstone particles of different sizes. According to the ASTM test standard [12], the maximum particle size in the compaction cylinder must not be greater than 1/3 of the inner diameter of the cylinder. The current test used a sorting sieve to allocate the stone particles into the following groups: 10–15 mm, 15–20 mm, 20–25 mm, and 25–30 mm (Figure 3).

Single-size particle samples and the mixed-size particle sample were both compacted in this experiment to study the effect of particle size and gradation on the results. Single-size particle samples were prepared from the 15–20 mm, 20–25 mm, and 25–30 mm particle groups. Mixed-size particle sample was prepared from a 1 : 1 : 1 : 1 mixture of 10–15 mm, 15–20 mm, 20–25 mm, and 25–30 mm particles. For all test schemes, stone particles with a total mass of 2000 g were charged into the compaction device. Table 1 shows the mass of particles with different sizes in each test scheme.

In order to study the influence of compaction level and loading speed on the test results, in this work, the

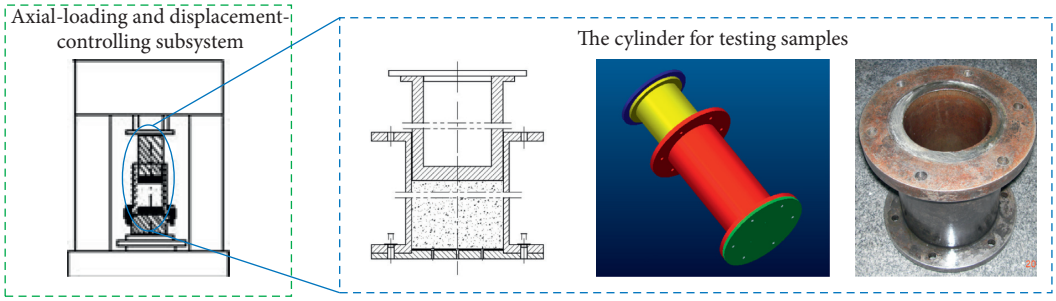

Figure 2: The compaction test system of crushed stone.

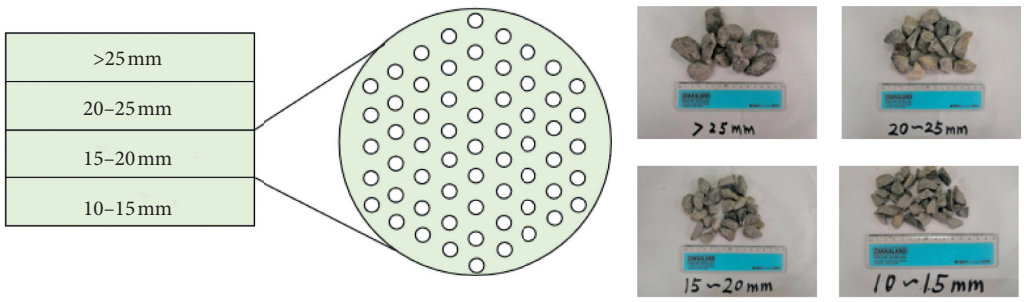

(a) (b)

Figure 3: The screen and rock particles.

Table 1: Particle mass of different samples.

Mass (g)		Particle size (mm)			
		10–15	15–20	20–25	25–30
Single size particle samples (mm)	25–30	0.0	0.0	0.0	2000.0
	20–25	0.0	0.0	2000.0	0.0
	15–20	0.0	2000.0	0.0	0.0
Mixed size particle sample	1 : 1 : 1 : 1	500.0	500.0	500.0	500.0

compaction level was tested at 10 mm, 20 mm, 30 mm, and 40 mm and the loading speed was tested at 1 mm/min, 2 mm/min, 4 mm/min, and 6 mm/min. All tests were performed in triplicate, and the average value was taken as the result to ensure the accuracy of the test results.

2.3. Experimental Procedure. Figure 4 shows the test process. The stone particles were thoroughly mixed and then charged into the compaction cylinder, after which the sample was gently compressed and the sample height was measured. The hollow piston and piston cap were then installed. The compaction device was placed in the lower chamber of the WDW-100D testing machine, and an initial load of 0.02 kN was applied. The reading of the scale paper was then recorded, and the sample height was calculated. Afterward, the compaction level was attained at the set loading speed. The crushed particles were then discharged and sorted into groups with a size of 0–2 mm, 2–5 mm, 5–10 mm, 10–15 mm, 15–2 0 mm, 20–25 mm, and 25–30 mm, respectively.

3. Results

Because various factors (particle size, gradation, and compaction level, etc.) were considered in the test, the following demonstrates the test result with 40 mm compaction and 2 mm/min loading speed as an example to illustrate the strength characteristics, particle breakage characteristics, and particle size changes.

3.1. Strength Characteristics. Figure 5(a) shows the force-time curves for samples subject to 40 mm compaction. The curves can be divided into two stages. The first stage corresponds to preliminary compaction. The curves of all samples superimpose. In this stage, particles came into contact with each other, and the internal pores of the

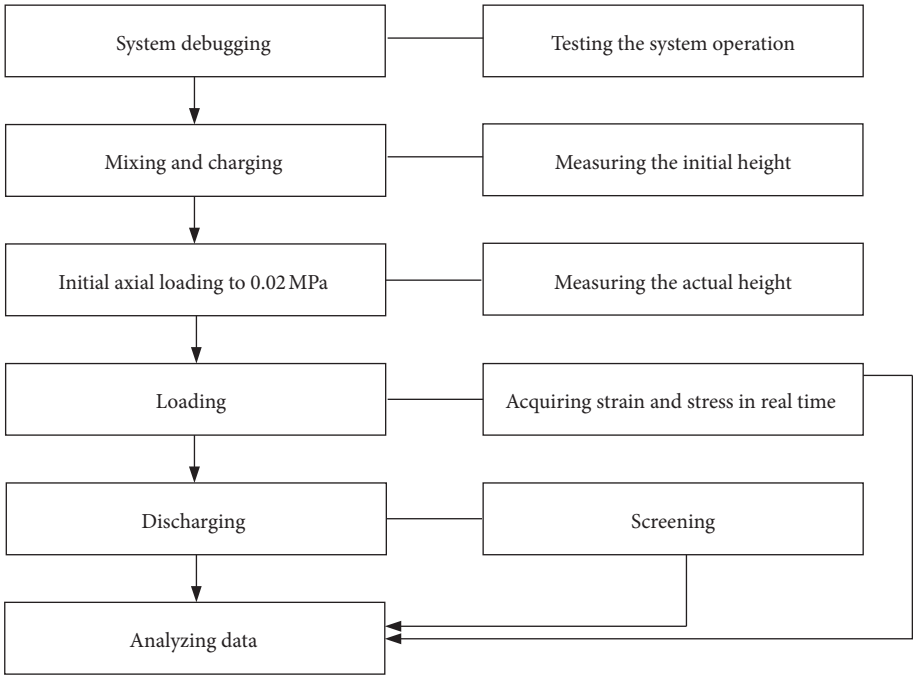

Figure 4: Test procedure.

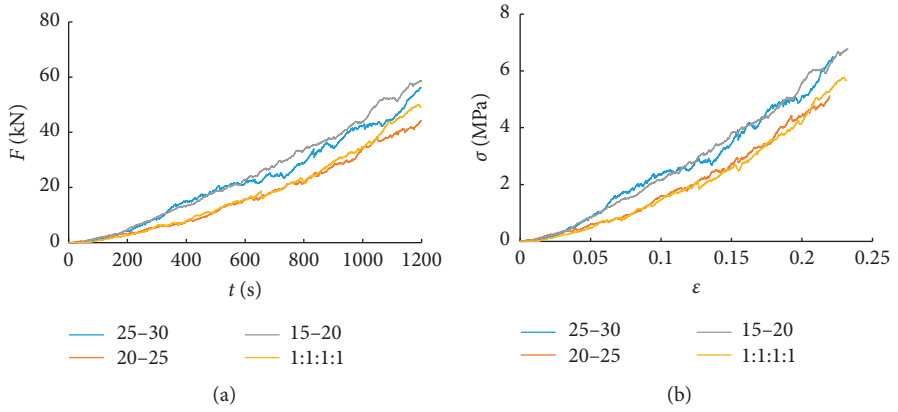

Figure 5: The force-time and stress-strain curves for samples subject to 40 mm compaction.

structure were reduced. The second stage corresponds to particle crushing and compaction, and the curves clearly differentiated as the particle size of the samples varied. Cycles alternating between compacting and crushing were clearly visible. The time in the second stage varied for samples with different particle sizes. In addition, particle size also affected the loading force. When the compaction level was 40 mm, the 15–20 mm particles required the largest force (58.48 kN), whereas the 20–25 mm particles required the smallest force (44.48 kN). However, the direct correlation between loading force and particle size was not verified in this study.

By comparison, the mixed size particle sample had the worst strength in the first stage of compaction and demonstrated higher strength than the 20–25 mm particles only at the end of the compaction test, but its strength was always lower than the other two samples.

Figure 5(b) shows the stress-strain curves of all samples with a 40 mm compaction. The curves show a similar trend to that of the force-time curves. The stress also varied with

the particle size of the sample. The 20–25 mm particles had a relatively low stress of 5.13 MPa, but the 15–20 mm particles had a higher stress of 6.75 MPa. In addition, larger particle sizes generally corresponded to earlier initiation of cracking. The stress-strain curves of single particle size samples were almost parallel, which indicated minimal difference in elastic modulus.

The mixed-size particle sample had a maximum stress of 5.74 Mpa, and its stress-strain curve largely overlapped to that of the 20–25 mm particles. Its initiation of cracking was slightly later compared with the 20–25 mm particle sample.

It can be seen from Figures 5(a) and 5(b) that fluctuation in both force and stress was the largest for 25–30 mm particles. It can be inferred that the larger particle size gives rise to greater particle crushing during compaction.

3.2. Particle Size Distribution after Compaction. The stability of the sample after compaction and crushing depends on the particle size distribution [13, 14]. Figure 6 shows the redistribution of particle size after the sample was loaded and crushed. It can be seen from the figure that for all samples, the structure after crushing still mainly consisted of the original large particles, and the total amount of secondary particles generated after loading accounted for less than 50%. The generated secondary particles did not impair but in fact enhanced the stability of the structure because smaller particles gradually filled the pores in the sample.

Figure 6 shows that the particle size distribution after crushing can be expressed analogously to the Talbot continuous gradation equation [15] as a power function of the particle size ratio ($d/d_{\max}$). Table 2 shows that after compaction, the continuous gradation sample has a larger coefficient of the particle size distribution function than the discontinuous gradation sample and the single particle size sample. In addition, for the single particle size sample after compaction, the coefficient of the particle size distribution function decreases with rising particle size.

As shown in Table 2, the particle size distribution of the sample after crushing can be expressed as

$$p(d) = a\left(\frac{d}{d_{\max}}\right)^{b} \times 100\%, \tag{1}$$

where coefficient a and the power exponent b are both related to the particle breakage characteristics of the particles. Therefore, the redistribution of particle size may be predicted based on the particle breakage characteristics of the sample.

4. Discussion

4.1. Characteristics and Calculation of Particle Breakage. Before compaction, particles are arranged in a disorderly manner with poor contact that is mainly point-to-point and point-to-surface [16–18]. The structure is constructed by large particles and relatively loose, with relatively large internal pores. As the axial stress increases, the pores are compressed or filled with small particles. Particle breakage becomes obvious, and some large particles are fragmented to produce secondary smaller particles, as seen in Figure 7. The changes in particle size distribution give rise to the relative displacement between particles as well as their rearrangement. Particles gradually enter stable surface-to-surface contact and meta-stable contact. It could be seen that the particle breakage characteristics and the change of particle size strongly affect the stability of the sample structure.

Quantitative indicators are needed to measure and analyze particle breakage [19–24]. Because it is difficult to test gradation during compaction, the current experiment only measured particle breakage after compaction was finished. Confining pressure and other factors in the compaction process were not considered. Particle breakage is thus quantified by B_g according to Marsal as follows [19]:

$$B_g = \sum \Delta W_k, \tag{2}$$

where ΔW_k is the difference in the content between particles of a certain size before and after compaction and B_g is the degree of particle breakage, calculated as the sum of particle content increment and expressed as a percentage.

4.2. The Influence of Particle Size and Gradation on Particle Breakage. As the particle size and gradation vary, particles are arranged very differently after the samples are charged in the test instrument, and the contact between particles also differs. As a result, particles are crushed in different ways during compaction. Hence, particle size and gradation both affect particle breakage [25].

Table 3 shows the difference in particle size content as well as the particle breakage for samples compacted to 40 mm at a loading speed of 2 mm/min. The particle breakage is above 43% for all single-size particle samples and about 20% for the mixed-size particle sample. That is, single-size particle samples are more severely crushed than the mixed-size particle sample. In single-size particle samples, particles are in rigid contact and more likely crushed after compaction. In contrast, small particles fill the pores between large particles to form semirigid contact in the mixed particle size sample. Particle breakage is thus less during compaction, and the sample has higher structural stability. It has been stipulated for the bedding course of roads that particle breakage must not be greater than 26% when the maximum particle size is less than 60 mm [26]. Therefore, in paving the bedding course, the crushed stone in the aggregate should not adopt a single particle size but use a mixed particle size.

4.3. The Effect of Compaction Level on Particle Breakage. Aside from particle size and gradation, the compaction level after loading also affects the particle breakage of samples. Samples were compacted to 10, 20, 30, and 40 mm and then sieved to determine the particle breakage. Table 4 lists the change in particle size content before and after compaction to different levels.

Figure 8 shows the relationship between particle breakage and compaction level for different samples. It can

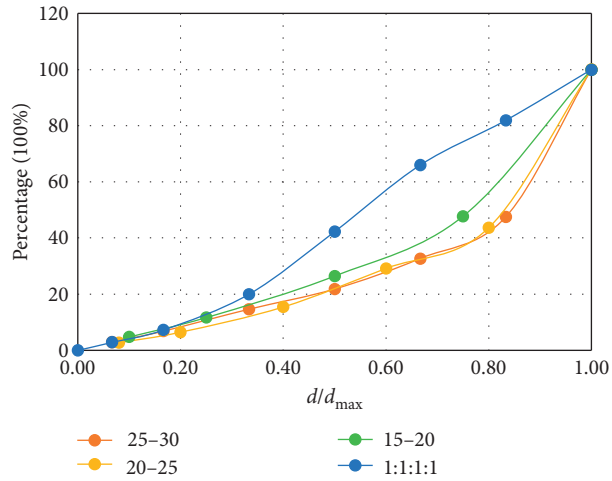

Figure 6: The redistribution of particle size after the sample was loaded and crushed.

Table 2: The particle size distribution functions.

Samples		Functions	R^2
Single-size particle samples (mm)	25–30	$p(d) = 62.688(d/d_{max})^{1.1987} \times 100\%$	0.9578
	20–25	$p(d) = 66.488(d/d_{max})^{1.3542} \times 100\%$	0.9635
	15–20	$p(d) = 76.463(d/d_{max})^{1.2683} \times 100\%$	0.9733
Mixed-size particle sample	1 : 1 : 1 : 1	$p(d) = 102.82(d/d_{max})^{1.3739} \times 100\%$	0.9917

Figure 7: The crushed rock particles after compaction.

be seen from Figure 8(a) that particle breakage increased with a rising compaction level for both single particle size samples and the mixed particle size sample. The slopes of the curves at different loading stages vary slightly. The compaction can be divided into four stages each with a 10 mm increment. In the first stage, the mixed particle size sample only had a low breakage of 3%, the 15–20 mm particles had a breakage of 9%, and the 20–25 mm and 25–30 mm particles had the highest breakage of 11%. In the second stage, the 20–25 mm particles had a breakage of 18%, much higher than that of the 15–20 mm particles (9%), 25–30 mm particles (6%), and the mixed particles (4.5%). In the third stage, the 25–30 mm particles showed a rapid rise in breakage to 22.8%, whereas the 15–20 mm and 20–25 mm particles both

Table 3: The particle breakage for samples with different particle size and gradation.

Samples		Particle size (mm)							B_g (%)
		0–2	2–5	5–10	10–15	15–20	20–25	25–30	
Single-size particle samples (mm)	25–30	2.95	3.89	7.79	7.22	10.85	14.85	−47.45	47.53
	20–25	2.70	3.75	9.01	13.72	14.51	−43.65	—	43.65
	15–20	4.75	6.94	14.76	21.31	−47.75	—	—	47.75
Mixed-size particle sample	1 : 1 : 1 : 1	2.87	4.41	12.75	−2.71	−1.29	−9.11	−6.92	20.02

Table 4: The particle size content and particle breakage for samples with different compaction levels.

Samples (mm)		Particle size (mm)							B_g (%)
		0–2	2–5	5–10	10–15	15–20	20–25	25–30	
25–30	10	0.24	0.16	0.28	1.56	2.08	6.94	−11.15	11.15
	20	0.56	0.70	1.80	2.60	3.55	7.86	−17.03	17.03
	30	1.57	2.35	5.23	5.33	7.05	18.31	−39.80	39.80
	40	2.95	3.89	7.79	7.22	10.85	14.85	−47.45	47.45
20–25	10	0.27	0.29	0.81	2.54	7.88	−11.75	—	11.75
	20	0.83	1.19	3.45	6.43	17.83	−29.63	—	29.63
	30	2.15	2.95	6.23	9.54	17.44	−38.28	—	38.28
	40	2.70	3.75	9.01	13.72	14.51	−43.65	—	43.65
15–20	10	0.49	0.28	1.47	6.77	−8.94	—	—	8.94
	20	1.07	1.28	3.83	11.61	−17.70	—	—	17.70
	30	1.70	2.39	7.45	15.96	−27.45	—	—	27.45
	40	4.75	6.94	14.76	21.31	−47.75	—	—	47.75
1 : 1 : 1 : 1	10	0.18	0.27	2.52	−2.53	−0.35	−0.09	0.00	2.97
	20	0.66	1.01	4.88	0.88	−1.17	−3.24	−3.00	7.42
	30	1.17	1.65	6.77	0.10	−0.96	−2.25	−6.43	9.69
	40	2.87	4.41	12.75	−2.71	−1.29	−9.11	−6.92	20.02

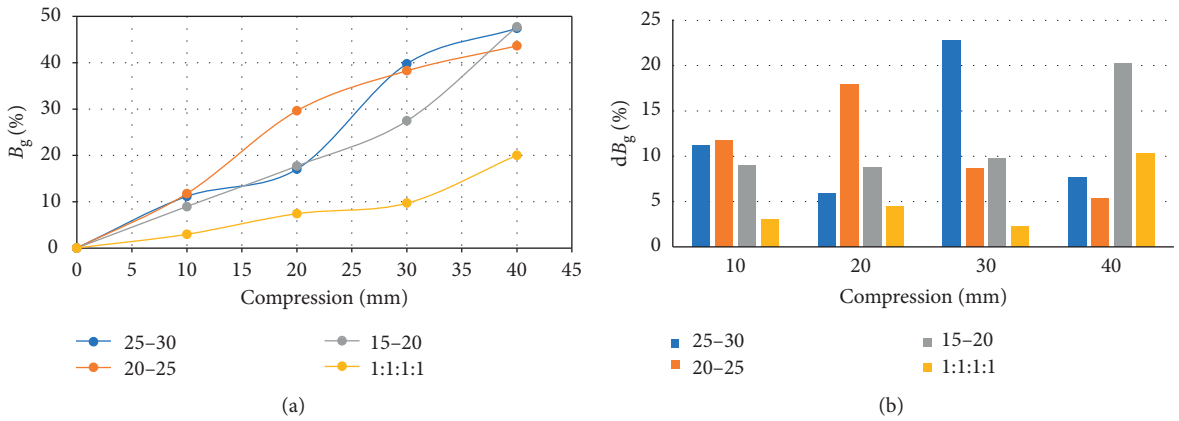

Figure 8: The relationship between particle breakage and compaction level.

had a breakage of about 9% and the mixed particles had a breakage of only 2%. In the fourth stage, the 15–20 mm particles gave the highest breakage of 20%, the mixed particles gave an enhanced breakage of 11%, the 20–25 mm particles gave a breakage of about 8%, and the and 25–30 mm particles gave only 5% breakage.

5. Conclusions

The current study on permeable roads helps build smart cities with sponge-like functionality to address urban flooding in Chinese cities caused by frequent heavy rainfall. Experiments on the compaction of crushed stone were

carried out by considering the impact of particle size and gradation to examine the strength and particle breakage characteristics of crushed stone and evaluate its use as the aggregate in the bedding course of permeable roads. The following can be concluded:

(1) The force-time curve can be divided into two stages, i.e., the preliminary compaction stage and the particle crushing and intensive compaction stage. The latter consists of an alternating cycle of compacting and crushing.

(2) The mixed particle size sample has no advantage compared with the single particle size samples with regard to strength because its initiation of particle cracking is much later during the compaction process.

(3) The particle size distribution after crushing can be described analogously to the Talbot continuous gradation equation. The coefficient and the power exponent are related to the particle breakage characteristics of the sample.

(4) Particle crushing commonly falls into four categories: complete crushing, complete rupture, partial damage, and surface grinding.

(5) Single particle size samples are subject to stronger particle breakage than the mixed particle size sample, and both the compaction level and the loading speed affect particle breakage. In view of appropriate regulations of the bedding course, the crushed stone aggregate for permeable roads should consist of particles of mixed size.

Data Availability

The data used to support the findings of this study are available from the author upon request.

Conflicts of Interest

The authors declare that they have no conflicts of interest.

Acknowledgments

The authors gratefully acknowledge the authors of the references. This work was supported by the National Natural Science Fund (51808481) and the Natural Science Foundation of Jiangsu Province of China (BK20170477).

References

[1] K. Yu, D. Li, H. Yuan, W. Fu, Q. Qiao, and S. Wang, ""Sponge city": theory and practice," *City Planning Review*, vol. 39, no. 6, pp. 26–36, 2015.

[2] J. Xu, X. Zhang, W. Lin, and H. Xu, "Evaluative methods on effect of disaster reduction for planning of intelligent sponge cities in perspective of drainage basin," *Urbanism and Architecture*, vol. 15, no. 15, pp. 17–21, 2018.

[3] T. Cai, "Application of water permeable materials in the construction of sponge city," *Shanxi Architecture*, vol. 46, no. 11, pp. 120-121, 2020.

[4] GB50400-2006, *Engineering Technical Code for Rain Utilization in Building and Sub-district*, Ministry of Construction of the PRC, Beijing, China, 2006.

[5] Y. Meng, T. Li, S. Wang, and Z. Fu, "Field survey and application analysis of infiltration performance of permeable pavements in Shanghai city," *China Water & Wastewater*, vol. 25, no. 6, pp. 29–33, 2009.

[6] D. Liu, "Construction type and road-related performance of permeable pavement of sponge city," *Jiangxi Building Materials*, vol. 25, no. 7, pp. 108-109, 2019.

[7] G. Lu, Z. Wang, P. Liu, D. Wang, and M. Oeser, "Investigation of the hydraulic properties of pervious pavement mixtures: characterization of darcy and non-darcy flow based on pore microstructures," *Journal of Transportation Engineering, Part B: Pavements*, vol. 146, no. 2, Article ID 04020012, 2020.

[8] G. Lu, L. Renken, T. Li, D. Wang, H. Li, and M. Oeser, "Experimental study on the polyurethane-bound pervious mixtures in the application of permeable pavements," *Construction and Building Materials*, vol. 202, pp. 838–850, 2019.

[9] X. Wang, "Analysis of factors influencing the strength of permeable pavement materials," *East China Highway*, vol. 42, no. 4, pp. 80-81, 2019.

[10] S. Borgwardt and Y. Chen, "Study on long term permeability of permeable concrete pavement brick pavement," *Building Block & Block Building*, vol. 15, no. 2, pp. 37–41, 2008.

[11] S. Borgwardt, "Long-term in-situ infiltration performance of permeable concrete block pavement," in *Proceedings of the 8th International Conference on Concrete Block Paving*, San Francisco, CA, USA, November 2006.

[12] ASTM International, *ASTM C39/C39M-15a, Standard Test Method for Compressive Strength of Cylindrical Concrete Specimens*, ASTM International, West Conshohocken, PA, USA, 2015.

[13] H. Kong, L. Wang, and H. Zhang, "Fractal and re-breakage behavior of the saturated rock granular material under-compaction," *Arabian Journal of Geosciences*, 2020.

[14] H. Kong, L. Wang, and H. Zhang, "The variation of grain size distribution in rock granular material in seepage process considering the mechanical-hydrological-chemical coupling effect: an experimental research," *Royal Society Open Science*, vol. 7, no. 1, Article ID 190590, 2020.

[15] A. N. Talbot and F. E. Richart, "The strength of concrete and its relation to the cement, aggregate and water," *Bulletin, University of Illinois Engineering Experiment Station*, vol. 11, no. 7, pp. 1–118, 1923.

[16] M. Cai, M. He, and D. Liu, *Rock Mechanics and Engineering*, Science Press, Beijing, China, 2002.

[17] Y. Gao, B. Zhang, W. Liu, and Y. Ai, "Experimental study on particle breakage behavior of rockfills in large-scale triaxial tests," *Rock and Soil Mechanics*, vol. 30, no. 5, pp. 1237–1240, 2009.

[18] X. Lei, Z. Yang, X. Zhang, Y. Tu, S. Liu, and Y. Hu, "Shear properties and rock block breakage characteristics of soil-rock mixtures," *Rock and Soil Mechanics*, vol. 39, no. 3, pp. 899–908, 2018.

[19] R. J. Marsal, "Large scale testing of rockfill materials," *Journal of the Soil Mechanics and Foundations Division*, vol. 93, no. 2, pp. 27–43, 1967.

[20] B. O. Hardin, "Crushing of soil particles," *Journal of Geotechnical Engineering*, vol. 111, no. 10, pp. 1177–1192, 1985.

[21] P. V. Lade, J. A. Yamamuro, and P. A. Bopp, "Significance of particle crushing in granular materials," *Journal of Geotechnical Engineering*, vol. 122, no. 4, pp. 309–316, 1996.
[22] I. Einav, "Breakage mechanics-Part I: theory," *Journal of the Mechanics and Physics of Solids*, vol. 55, no. 6, pp. 1274–1297, 2007.
[23] S. Wei, J. Zhu, Q. Qian, and F. Li, "Particle breakage of coarse-grained materials in triaxial tests," *Chinese Journal of Geotechnical Engineering*, vol. 31, no. 4, pp. 533–538, 2009.
[24] H. Liu, H. Qin, Y. Gao, and Y. Zhou, "Experimental study on particle breakage of rockfill and coarse aggregates," *Rock and Soil Mechanics*, vol. 26, no. 4, pp. 562–566, 2005.
[25] J. Wu, M. Feng, X. Mao et al., "Particle size distribution of aggregate effects on mechanical and structural properties of cemented rockfill: experiments and modeling," *Construction and Building Materials*, vol. 193, no. 12, pp. 295–311, 2018.
[26] Z. He and X. Yang, *Subgrade and Pavement Engineering*, Chongqing University Press, Chongqing, China, 2015.